Crystallization and Morphological Features of Syndiotactic/Atactic Polystyrene Blends at Low Temperatures near Glass Transition

Chi Wang,* Chang-Chun Lin, and Chia-Pin Chu

Department of Chemical Engineering, National Cheng Kung University, Tainan, Taiwan 701, Republic of China

Received May 23, 2006; Revised Manuscript Received September 24, 2006

ABSTRACT: Crystallization and morphological features of syndiotactic/atactic polystyrene (sPS/aPS) mixtures with a constant weight ratio of 5/5 but different weight-average molecular weights (MW) of aPS, i.e., 1880K (aPS-U), 100K (aPS-H), 4.3K (aPS-M), and 1.3K (aPS-L), have been investigated. For these athermal blends cold-crystallized at temperatures near the glass transition, MW effects of aPS on the spherulitic growth rates (G) have been examined using small-angle light scattering to detect the structural evolution at various isothermal temperatures (T_c). In addition, the crystallinity and segregation morphology of the cold-crystallized samples were also acquired using Fourier transformation infrared spectroscopy (FTIR) and scanning electron microscopy, respectively. Compared with neat sPS at a given T_c, the retardation of G was evident in the sPS/aPS-U and sPS/aPS-H blends, whereas G was increased in the other two blends. By considering both effects of dilution and T_g variation, a master curve of the normalized G vs $T_c - T_g$ was successfully constructed for the neat sPS and all blends except the sPS/aPS-L. For the sPS/aPS-L blend, an extra energy was required for the sPS demixing and transportation to the crystal growing front, resulting from the enhanced mixing entropy associated with the aPS oligmers used. Owing to the high mobility of aPS-L chains, moreover, the sPS/aPS-L blend exhibited interspherulitic segregation morphology, whereas the sPS/aPS-U blend showed an interlamellar segregation at low 120−160 °C, but a mixed segregation of interlamellar/interfibrillar morphology at 160−200 °C. Under optical microscope observations on the crystallized samples, a regularly bicontinuous structure with periodic wavelength of about 2−5 μm, depending on T_c, was found for all blends as well as the neat sPS, suggesting the occurring of liquid−liquid (SD-like) phase separation coupled with crystallization. Regardless of the T_c used, the signature of SD-like structure was always preserved within the developed spherulites; its wavelength was smaller than the spherulitic diameter (6−10 μm). For all crystallized blends, T_c dependence of the Hv scattering invariant (Q_{Hv}) exhibited a pronounced minimum and the corresponding temperature (T_{min}) was relevant with the chain mobility in the blends. Despite the differences in T_c (100−180 °C) and MW of aPS (1.3−1880K) used, FTIR results showed that the blend crystallinity was relatively unchanged, being ca. half of that for the pristine sPS, and the crystal modification was either mesomorphic or α-form crystals. These facts suggest that the Q_{Hv} minimum is attributed to the irregular packing of lamellar crystallites within spherulites, resulting from the comparable competition between the phase separation and cold crystallization at T_{min}. In contrast, phase separation and cold crystallization become the dominant phase transition respectively at the lower and higher temperature regimes, giving rise to the development of more ordered symmetry within spherulites.

1. Introduction

Syndiotactic polystyrene (sPS) is a high performance semicrystalline polymer which is increasingly used in practical applications requiring its high-temperature and polymorphic properties. On the other hand, atactic polystyrene (aPS) is amorphous and glassy. By blending, favorable properties and versatile morphologies can be obtained for the desirable application. The binary sPS/aPS mixtures have been shown to be miscible in the liquid state.[1−4] For melt crystallization, the overall crystallization rate and crystal growth rate of the sPS/aPS blend are decreased in comparison with those for the neat sPS.[4−7] Molecular weight (MW) effects of aPS on the morphologies and crystallization kinetics of sPS have been systematically studied.[4,7,8] Depending on the aPS mobility and the crystal growth rate of sPS in the blends, it is generally recognized that three distinct morphologies can be distinguished. The amorphous aPS component is rejected from the growing sPS lamellae to reside in the interlamellar (IL), interfibrillar (IF), or interspherulitic (IS) regions, ranging accordingly from the smallest to the largest segregation scale, or some combination of these. Thus, in addition to the crystallization conditions, the placement of aPS component is closely related to aPS MW used. In other words, careful selection of the MW of aPS can lead to various blend morphologies, which in turn give rise to different blend properties.

Previous articles have mainly focused on the kinetics and morphology of the sPS/aPS blends crystallized at high temperatures by quenching from the molten state.[4−8] In contrast, crystallization kinetics at low temperatures near glass transition has not been reported yet. To complement and compare with the melt-crystallization results,[7,8] cold crystallization was carried out in this study. Although polarized optical microscopy (POM) is frequently conducted to measure the spherulitic growth rate, difficulties are often encountered due to the magnification limit when the morphological entity is too small to be resolved. Small spherulites with a diameter of ca. 8 μm are readily found in the cold-crystallized sPS/aPS blends, leading to the infeasibility of POM for measuring the spherulitic growth. Instead, small angle light scattering (SALS) provides a feasible route to monitor the growth of tiny sPS spherulites. In this work, SALS has been extensively performed to determine the growth rates of sPS spherulites in the sPS/aPS blends with a wide MW range (1.3−1880K) of aPS diluents. By varying the aPS MW from the

* Corresponding author. Fax: +886-6-2344496. Telephone: +886-6-2757575 Ext 62645. E-mail: chiwang@mail.ncku.edu.tw.

10.1021/ma061159k CCC: $33.50
Published on Web 12/02/2006

oligomers to ultrahigh MW chains, a significant difference in the aPS chain mobility occurs, resulting in profound morphologies developed in the blend. Effects of aPS MW on the crystallization of sPS and blend microstructure, i.e., the crystal forms, segregation type, and lamellae, are discussed as well.

During the course of sPS/aPS cold crystallization, we observed the bicontinuous structure with a characteristic length smaller than the spherulitic diameter, suggesting the coexistence of two transitions i.e., liquid−solid (L−S) cold crystallization and liquid−liquid (L−L) phase separation. For a binary blend, coexistence of L−S and L−L phase transitions has been also observed in other system.[9−13] Interestingly, a similar morphology with interconnected domains embedded within the well-defined spherulites was also found in the neat sPS sample.[14] For this single-component sPS, it was suggested that conformation ordering coupled with density fluctuation was the main event to account for the spinodal decomposition (SD) phase separation involving two phases;[15,16] one possesses the preferential conformation for subsequent crystallization, while the other remains amorphous due to the random conformation. Since sPS and aPS have the same constituent monomer but different stereoregularities, absence of any specific interaction between them is expected, making this athermal blend a good candidate for studying the stereo-regularity effect on the phase separation. Because of the structure similarity, the refractive indexes of sPS and aPS are close to each other, giving rise to the difficulty in studying the structure evolution of phase separation and L−L phase boundary using the cloud-point method (either by light scattering or optical microscopy) based on the turbidity measurements. Previously, the miscibility of sPS/aPS-H blends at 300 °C has been confirmed on the basis of enthalpy relaxation via the DSC study, but the plausible existence of upper critical solution temperature (UCST) phase boundary has not been reported yet. Using a double temperature jump experiment,[17] the phase-separated morphology of isotactic/atactic polypropylene (iPP/aPP = 5/5) blends was preserved after the crystallization of iPP. The UCST of iPP/aPP blends was found to lie below 155 °C, which was lower than the melting temperature of iPP. Similar experiments have been conducted in our preliminary studies on the miscibility of sPS/aPS by quenching the sPS/aPS melt at 300 °C to 280−290 °C for holding 4 h, followed by crystallization at 260 °C. We found that the growth rate at 260 °C and the developed spherulites were identical to those without having the intermediate-temperature annealing. It led to the conclusion that phase separation did not take place in the sPS/aPS blends at temperatures above 280 °C. Although the apparent melting temperature of the sPS/aPS blends was typically at ∼270 °C, the derived equilibrium melting temperature was ca. 291 °C on the basis of linear Hoffman−Weeks plot.[18] On the basis of these facts, it is likely that the L−L binodal curve is buried under the L−S transition. Since there is no energy barrier required for SD phase separation, phase separation is expected to precede crystallization in the unstable regime; crystallization takes place within the already phase-separated medium. For sPS/aPS blends melt-crystallized at temperatures lower than 280 °C, the phase-separated structure and the nonequilibrium UCST are difficult to be detected due primarily to the subtle phase variation and the plausible structure rearrangement associated with the high chain mobility at the crystal growing front. In other words, the melt-crystallized sPS/aPS blends often give a spherulitic morphology in the absence of SD signature.[7,8] In contrast with melt crystallization, limited segmental mobility is expected in the sPS/aPS blends at low temperatures ($T_g \sim T_g + 50$ °C), which in turn prohibits significant structure rearrangement at the phase boundary, resulting in the plausible preservation of SD structure. Thus, thermal induction from the glassy state could provide useful information for understanding the relative relevance of individual phase transitions, which is not feasible for the corresponding process induced from the melt. This paper concerns the crystallization kinetics and morphological features developed for sPS/aPS blends induced by cold crystallization. Our objective was 2-fold. First, we explore the MW effects of aPS diluents on the activation energy of sPS segmental mobility at the crystal growing front during cold crystallization. Second, we wish to clarify the morphology resulted from the interplay between L−L phase separation and L−S cold crystallization.

Table 1. Glass Transition Temperature, Weight Average Molecular Weight and Polydispersity Index of PS Used in This Study

	M_w (kg/mol)	M_w/M_n	T_g (°C)
sPS	200[a]	∼2.0	95.0
aPS-U	1880[a]	∼1.1	103.5
aPS-H	100[b]	∼2.2	99.9
aPS-M	4.3[b]	∼1.6	79.9
aPS-L	1.3[b]	∼2.2	28.7

[a] Provided by the supplier. [b] Measured by gel permeation chromatography using aPS standards.

2. Experimental Section

The molecular characteristics of the polymers used are tabulated in Table 1. sPS pellets were obtained from Dow Chemical Co. and aPS samples with different MW ranging from 1.3K to1880K were purchased from Aldrich Co. In this work, sPS/aPS-U, sPS/aPS-H, sPS/aPS-M, and sPS/aPS-L denoted the sPS blends mixed with aPS-U, aPS-H, aPS-M, and aPS-L, respectively. To prepare sPS/aPS-U and sPS/aPS-H blends with 5/5 weight ratio, solution blending was conducted by dissolving equal amount of both components in *o*-dichlorobenzene at 140 °C for 2 h, followed by pouring the homogeneous solution into a 20-fold excess of methanol. To remove the residual solvents, the collected precipitates were dried at a temperature lower than its glass transition in a vacuum until constant weight (ca. several days). Instead of coprecipitation, however, a casting method was applied for the sPS/aPS-M and sPS/aPS-L blends to avoid the dissolution of low MW species of aPS-M and aPS-L in the methanol during blend precipitation. Thus, the homogeneous solution was cast onto glass dishes and solvent evaporation was carried out under a vacuum for several days. Amorphous thin films (∼20 μm thick) were obtained by holding the as-prepared blends at 300 °C for 10 min, followed by quenching into liquid nitrogen. The quenched films were transparent and featureless under scanning electron microscopy observations. Wide-angle X-ray diffraction patterns showed no trace of crystallinity in these films. The amorphous state of these films was also ascertained by the absence of the absorbance band at 1222 cm^{-1} under Fourier transformation infrared spectroscopy (FTIR, Perkin-Elmer, Spectrum one). The band at 1222 cm^{-1} was assigned to the all-trans (T4) conformation in the sPS crystals and its intensity was relevant with the crystallinity degree developd.[19] On the basis of above facts, the as-obtained films frozen from the miscible state (300 °C) did not have time enough to evolve to a more stable thermodynamic state. The quenched film was placed in a hot stage (Linkam THMS600) and heated at a rate of 100 °C/min to the predetermined crystallization temperature (T_c) for isothermal crystallization. Using a vertical setup for SALS apparatus consisting of a 4 mW polarized He/Ne laser light, analyzer, and a highly sensible CCD camera (Apogee, A1) as the detector, time-resolved SALS were carried out under Hv polarization mode to trace the evolution of anisotropy fluctuation during cold crystallization. To observe the detailed morphology directly, a POM (Leica, DMLP) equipped with phase contrast lens was used. The relative crystallinity developed at the selected T_c was determined using FTIR in terms of the reduced factor obtained from the peak area ratio of 1222 to 1601 cm^{-1} bands

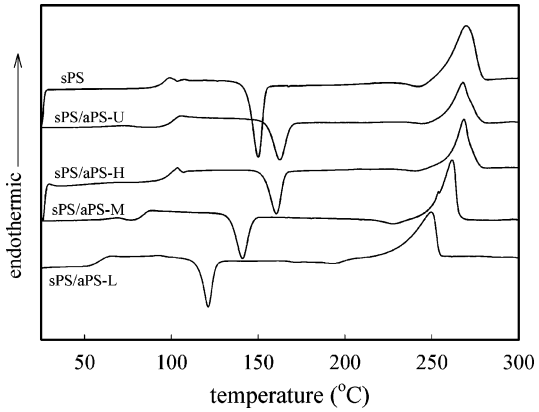

Figure 1. DSC heating traces on the melt-quenched sPS/aPS blends (heating rate: 10 °C/min).

Table 2. Thermal Properties of Amorphous Melt-Quenched sPS/aPS Blends

	T_g (°C)	$T_{c,max}$ (°C)	ΔH_c (J/g)	ΔH_m (J/g)	T_m (°C)	T_m^o (°C)[a]
neat sPS	95.08	150.23	16.31	28.35	269.97	281.0
sPS/aPS-U	100.82	162.53	11.34	15.80	267.93	281.0
sPS/aPS-H	98.30	160.40	10.91	18.96	268.35	280.8
sPS/aPS-M	83.55	141.03	11.50	20.40	261.83	277.3
sPS/aPS-L	58.50	120.00	9.02	20.90	250.20	269.3

[a] Equilibrium melting temperature for α-form sPS, estimated from the Flory−Huggins equation with interaction parameter $\chi = 0$.

after appropriate peak separations. The conformationally insensitive band at 1601 cm^{-1} which is attributed to the benzene ring stretching vibrations[19,20] was used to account for the variations in sample thickness. Morphologies of the sPS lamellar stacks and the segregated aPS domains were observed using SEM (Hitachi, S4100). Prior to SEM observation, the crystallized blends were etched using amyl acetate to wash away the aPS component. The etching procedure followed the method proposed by Kit and Schultz.[21] Thermal analyses on the amorphous melt-quenched blends were performed using differential scanning calorimetry (Perkin-Elmer DSC7) at a heating rate of 10 °C/min to obtain the dynamics of cold crystallization. Prior to measurements, the temperature and fusion enthalpy were calibrated using In and Pb standards. Nitrogen gas was circulated around the sample pan to prevent thermal degradation.

3. Results and Discussion

3.1. Dynamic Cold Crystallization and Melting. Figure 1 shows the DSC heating thermograms of the neat sPS as well as the blends. The measured thermal properties are displayed in Table 2. All the blends showed single glass transition. For neat sPS, the glass transition temperature (T_g) is ca. 95.08 °C and an exothermic enthalpy (ΔH_c) of 16.31 J/g associated with cold crystallization with a peak temperature ($T_{c,max}$) located at 150.23 °C is observed, followed by the crystal melting (T_m) at 269.97 °C with a melting enthalpy (ΔH_m) of 28.35 J/g. For the sPS/aPS-U, sPS/aPS-H, sPS/aPS-M, and sPS/aPS-L blends, the measured T_g is in agreement with the prediction by the Fox's equation. Judging by the apparent T_g reduction to 58.5 °C, the chain mobility of sPS/aPS-L blends is significantly enhanced due to the addition of low MW of aPS-L. Because of the reduced mobility as well as dilution effect, addition of aPS-U or aPS-H leads to the retardation of sPS crystallization, as evidenced by the increasing $T_{c,max}$ to 162.53 or 160.40 °C, respectively. For aPS-M and aPS-L blends, however, the mobility effect outweights the dilution effect, exhibiting a lower $T_{c,max}$ at 141.03 and 120.0 °C, respectively. In other words, crystallization of sPS is promoted by the addition of aPS-M or aPS-L as it occurs

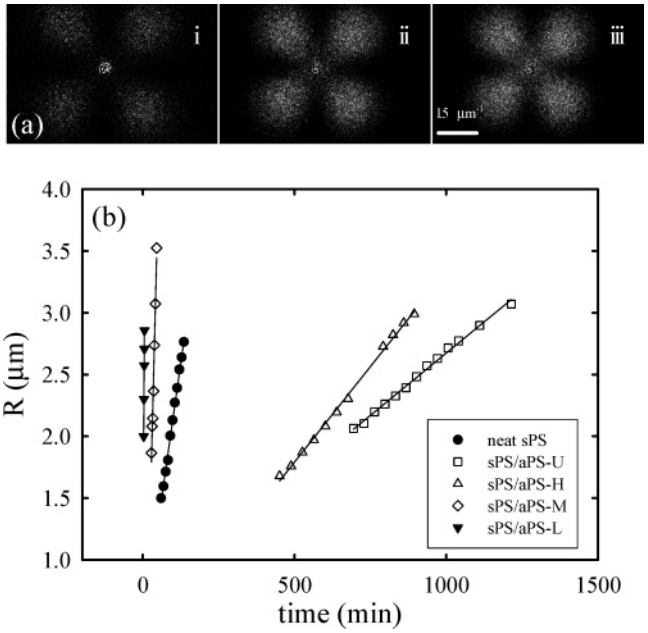

Figure 2. (a) Typical time evolution of Hv scattering patterns for sPS/aPS-U blends cold-crystallized at 120 °C for (i) 780, (ii) 1040, and (iii) 1390 min. (b) Plots of spherulitic radius vs time for samples cold-crystallized at 120 °C.

at a lower temperature with respect to neat sPS. For all the blends as well as the neat sPS, it is worth to noting that the crystallization enthalpy is lower than the subsequent melting enthalpy, suggesting the reorganization of sPS chains within the crystalline phase during the heating scan. In fact, mesomorphic sPS crystals are found during dynamic cold crystallization, and subsequent heating will improve the perfection of sPS crystals, giving rise to the melting of α-form (or mixed) crystals at T_m. Compared to the neat sPS, the increase in the normalized melting enthalpy, $\Delta H_m/\phi_{sPS}$ (ϕ_{sPS} is the volume fraction of sPS), for the blends may be related to an improved perfection of sPS crystals as well. As seen in Table 2, T_ms of the sPS/aPS-U and sPS/aPS-H blends are slightly lower than that of neat sPS, whereas apparent T_m depression is observed for the sPS/aPS-M and sPS/aPS-L blends. In general, the melting temperature of a crystalline polymer is affected by thermodynamic factors as well as morphological parameters, e.g., lamellar thickness (l_c). The thermodynamic factor refers to the depression of equilibrium melting temperature (T_m^o) due to the presence of aPS diluents. Since there is no specific energy interaction between sPS and aPS components for this athermal blend, T_m^o of the sPS/aPS blends can be estimated using the Flory−Huggins equation with $\chi \sim 0$, and the derived values are also tabulated in Table 2 assuming the formation of α-form crystals. Addition of low MW aPS-L gives rise to a pronounced decrease in T_m^o, resulting from the significant increase in the entropy of mixing. On the basis of the Gibbs−Thomson equation, l_c of the dynamically crystallized blends could be derived. With respect to the neat sPS, a pronounced reduction of l_c was observed for the sPS/aPS-L, suggesting that the dual effects lead to a significant lowering of T_m.[8]

3.2. Cold Crystallization Kinetics of sPS/aPS. Analysis by Spherulitic Growth Rates. When crystallized from the glassy state, all sPS/aPS blends developed spherulitic morphologies as revealed by SALS which exhibited the typical four-leaf-clover patterns under the Hv configuration. Typical evolution of Hv patterns of sPS/aPS-U crystallized at 120 °C is shown in Figure 2a. A scattering maximum was observed when the one-dimensional Hv scattering intensities at an azimuthal angle 45°

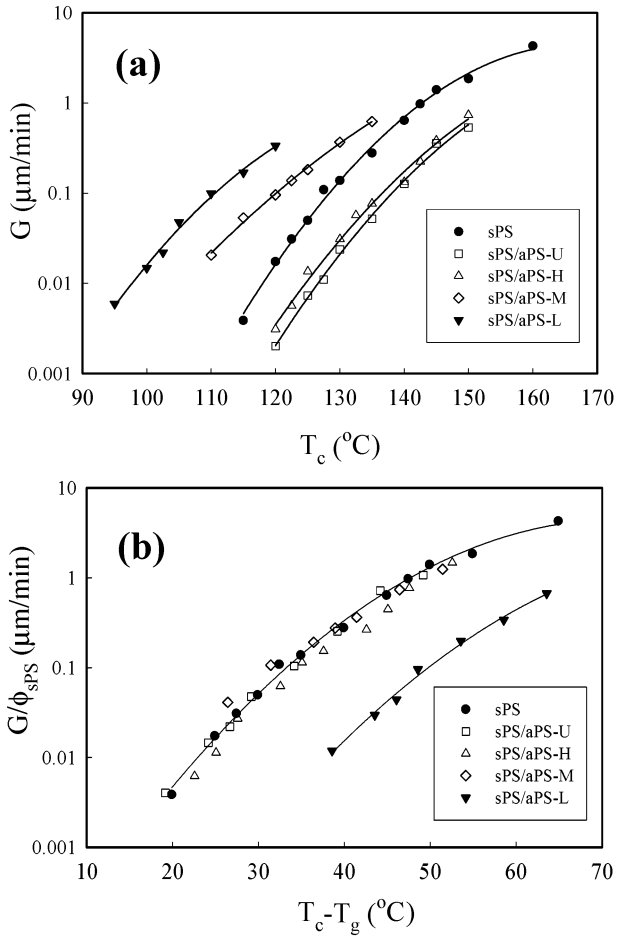

Figure 3. Spherulitic growth rates of sPS in the blends, (a) T_c dependence of G, (b) $T_c - T_g$ dependence of the normalized G. ϕ_{sPS} is the volume fraction of sPS.

were plotted against the scattering vector q ($=4\pi(\sin\theta)/\lambda$, where θ is the scattering angle and λ is the wavelength of laser light). To trace the evolution of spherulitic development, the change of Hv intensity profiles with elapsed time t_c during isothermal crystallization was recorded. The average radius (R) of growing spherulites at t_c was estimated by the formula expressed by[22] $R = 4.08/q_m$, where q_m is the position of the scattering maximum. Therefore, the spherulitic growth rate (G) at the given T_c was determined from the liner slope of $R-t_c$ plots, Figure 2b. Meanwhile, the Vv scattering patterns exhibit positive birefringence characteristic. Under POM observation, spherulite features are readily found; most of them are positively birefringent but the existence of spherulites with negative birefringence is also sporadically detected. The origin to render the difference in the birefringence characteristics is ascribed to the crystalline orientation within the spherulites.[7] Figure 3a shows the variation of G with T_c for the blends as well as the neat sPS. The measured G was increased by increasing T_c. When crystallization took place at temperatures higher than $T_{c,max}$ (as tabulated in Table 2), the spherulitic growth was too fast to be followed through the evolution of Hv scattering patterns. Compared with neat sPS, the retardation of G was obvious in both aPS-U and aPS-H blends, resulting from a dual effect of dilution and T_g elevation. In contrast, sPS growth rate was increased by addition of the low MW aPS components (either M or L), indicating that the dilution effect was overwhelmed by the enhanced molecular mobility due to the T_g lowering. To consider both effects on the measured G, Figure 3b shows the $T_c - T_g$ dependence of the normalized G with sPS volume fraction. It is of interest to

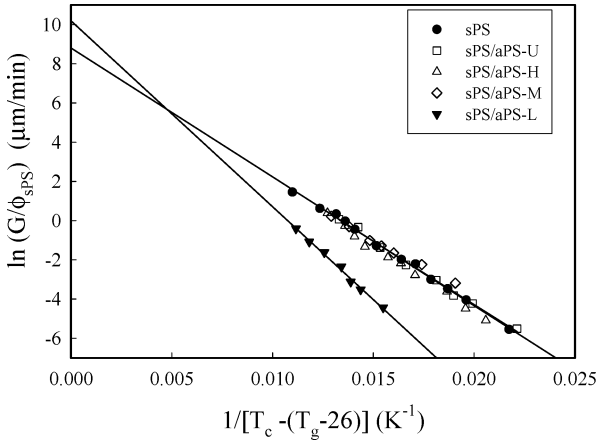

Figure 4. Determination of kinetics parameters for sPS/aPS blends on the basis of growth rate results.

observe the superposition of all blend data, except sPS/aPS-L, with the neat sPS results to form a master curve, suggesting a similar growth kinetics involved. On the other hand, a distinct kinetics is expected for the sPS/aPS-L blend since a vertical drop from the master curve is evident. A lower G/ϕ_{sPS} value is obtained for the sPS/aPS-L blend at a given $T_c - T_g$ despite the fact that its overall blend mobility is higher (Table 2). Thus, it could be concluded that it is the sPS mobility alone, not the overall blend mobility, that plays the key role during cold crystallization. Similar conclusion was also obtained previously from the melt crystallization results.[8]

When crystallization takes place from the glassy state, nucleation of stable nuclei is fast but the viscosity of sPS/aPS blends is rather high, leading to a diffusion control process. The activation energy for the sPS diffusion is better described by the WLF type for T_c not far from T_g ($T_g < T_c < T_g + 100$ °C). The T_c dependence of G for a blend can be expressed by eq 1.

$$G = \phi_{sPS} G_o \exp\left[\frac{-\Delta E_{WLF}}{R(T_c - T_\infty)}\right] \quad (1)$$

where G_o is a constant, ΔE_{WLF} is the WLF-type activation energy for transport of segments to the crystallization site, and T_∞ is the ceasing temperature below which the movement of polymer chains is infeasible. T_∞ is generally expressed as $T_g - C$, where C is a constant depending on the chain characteristics. For the neat sPS, the best-fitted C value is $\sim$ 26 K,[14] which is close to that for the neat iPS, $\sim$ 30 K.[23] According to eq 1, the spherulitic growth rate is dependent upon the magnitude of $T_c - T_\infty$. From the plots of ln G vs $1/(T_c - T_\infty)$ as shown in Figure 4, ΔE_{WLF} values were derived from the slopes by assuming a constant C value (26 K) for all the blends studied. Despite the wide range of aPS MW (4.3K−1880K) used, the effect of aPS MW on the ΔE_{WLF} and G_o for crystallization is negligible. The derived ΔE_{WLF} and G_o are 5.4 kJ/mol and 6.6 μm/min respectively, which are the same as those for the neat sPS.[14] In other words, there is no distinguished variation for sPS segmental diffusion provided that relatively high MW aPS chains are used. In contrast, addition of the extremely low MW of aPS-L gives rise to higher values of ΔE_{WLF} and G_o (7.9 kJ/mol and 26.7 μm/min correspondingly), leading to a different kinetics for cold crystallization. It should be noted that the entropy of mixing is pronounced in the sPS/aPS-L blend due to the low MW aPS used. The extra energy required for the sPS/aPS-L blend seems relevant to the additional energy barrier for sPS demixing from the "liquid pool" prior to its diffusion

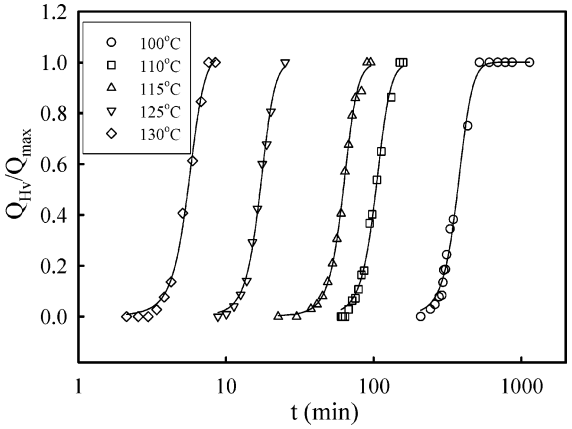

Figure 5. Q_{Hv} evolution of sPS/aPS-M blends cold-crystallized at various T_c.

to the crystal growth front. A similar trend was also obtained for sPS/aPS blends crystallized from the molten state.[7,8]

Analysis by Scattering Invariant. In addition to the scattering peak for determining the spherulitic size, crystallization kinetics is also frequently discussed in terms of the integrated scattering intensity, i.e., the invariant Q_{Hv} defined by[24]

$$Q_{Hv}(t) = \int_0^\infty I_{Hv}(q,t)q^2\,dq \cong \phi_{sp}(\delta_{cr}{}^o\phi_{c,sp}P_2)^2 \qquad (2)$$

where ϕ_{sp} is the volume fraction of spherulites, $\phi_{c,sp}$ is the volume fraction crystallinity within the spherulite, $\delta_{cr}{}^o$ is the intrinsic anisotropy of pure crystals and P_2 is a Hermans-type orientation function describing the lamellar orientation with respect to the radius of the spherulite. Prior to spherulitic impingement, the variations of $\phi_{c,sp}$, $\delta_{cr}{}^o$, and P_2 are assumed to be negligible during cold crystallization, leading to the assumption that $Q_{Hv}(t)$ should increase linearly with ϕ_{sp}. Thus, time-resolved Hv scattering invariant approach is also capable of detecting the crystallization kinetics together with the Avrami equation as follows,[25,26]

$$Q_{Hv}(t)/Q_{max} = 1 - \exp[-k(t - t_o)^n] \qquad (3)$$

where k is the overall crystallization rate constant, n is the Avrami component, t_o is the induction time of crystallization process, and Q_{max} is the invariant for complete crystallization. Figure 5 shows the time evolution of normalized Q_{Hv} for sPS/aPS-M blends crystallized at various T_c. Other blends displayed a similar trend. The crystallization half-time, $t_{1/2}$, is defined as the time required for the system to reach one-half of the relative conversion ($Q_{Hv}/Q_{max} = 0.5$). It is evident that both t_o and $t_{1/2}$ are significantly reduced at high T_c, suggesting a fast crystallization process at high T_c. A simple relation between these Avrami parameters is expressed by $(\ln 2/k)^n = 1/t_{1/2} \sim G$. Because of its convenient derivation, $1/t_{1/2}$ is an appropriate parameter to describe the relative rate of crystallization process.[4,14] On the basis of eq 3 from a correlation of $\ln[-\ln(1 - Q_{Hv}/Q_{max})]$ vs $\ln(t - t_o)$, the derived Avrami exponent is ~3.0 for all the blends as well as the neat sPS, suggesting three-dimensional growth of sPS spherulites with heterogeneous nucleation. A similar deduction for the melt-crystallized sPS/aPS samples has also been obtained previously.[7] The MW effect of aPS on the time evolution of Q_{Hv} is shown in Figure 6 for the blends crystallized at 120 °C. From the sigmoidal crystallization curves, $t_{1/2}$ and t_o are found to increase with increasing aPS MW, indicative of the retardation of overall crystallization rate. On the basis of $t_{1/2}$ results together with eq 1, the ΔE_{WLF} value for each blend could also be determined from the slope as shown in Figure 7. The calculated ΔE_{WLF} value for the sPS/aPS-L blend was 8.7 kJ/mol, which was still larger than other blends having the same ΔE_{WLF} (ca. 5.1 kJ/mol). In respect to previous findings obtained from growth-rate data (Figure 4), good agreement was reached, suggesting the consistency either using G or $t_{1/2}$ results for the kinetic analysis of cold crystallization. Compared with the other blends, the larger ΔE_{WLF} in the sPS/aPS-L blend essentially gives rise to a distinct morphology of aPS-L segregation as revealed by SEM, which will be discussed in section 3.4.

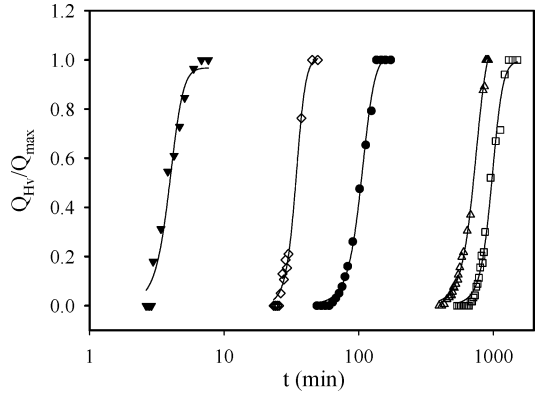

Figure 6. Comparison of Q_{Hv} evolution of sPS/aPS blends cold-crystallized at 120 °C. The symbols used for the blends are the same as those in Figure 3.

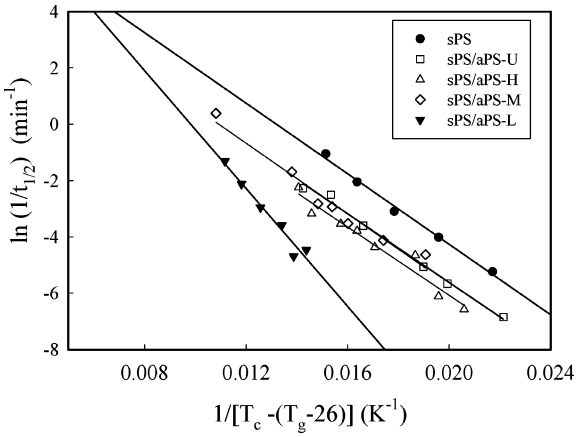

Figure 7. Determination of activation energy for sPS chain mobility on the basis of crystallization half-time obtained from Q_{Hv} evolution.

3.3. Structure Developed from Cold Crystallization. After complete crystallization at various T_c, all crystallized blends were characterized at room temperature using SALS, OM, FTIR and SEM to reveal the structure developed. Typical optical micrographs of blends crystallized at different T_c are shown in Figure 8, in which small spherulites of a diameter of ca. 7 μm are seen with cross-polarization, but a modulated structure reminiscent of spinodal decomposition (SD) is identified under bright-field observation. Because of the low phase contrast between sPS and aPS components, conventional methods of determining the time evolution of structure factor are not readily applicable. The dotted circles in the images on right column are for the eye-guide at the same region as those in the left column. For all the cold-crystallized blends studied, the bicontinuous structure is prevailing regardless of T_c used. In addition, it is of significance to observe the interconnected domains developed in the neat sPS as well.[14] It indicated that the SD-like structure was locked in by the crystallization of sPS, which was similar to some other systems reported previously.[9−11]

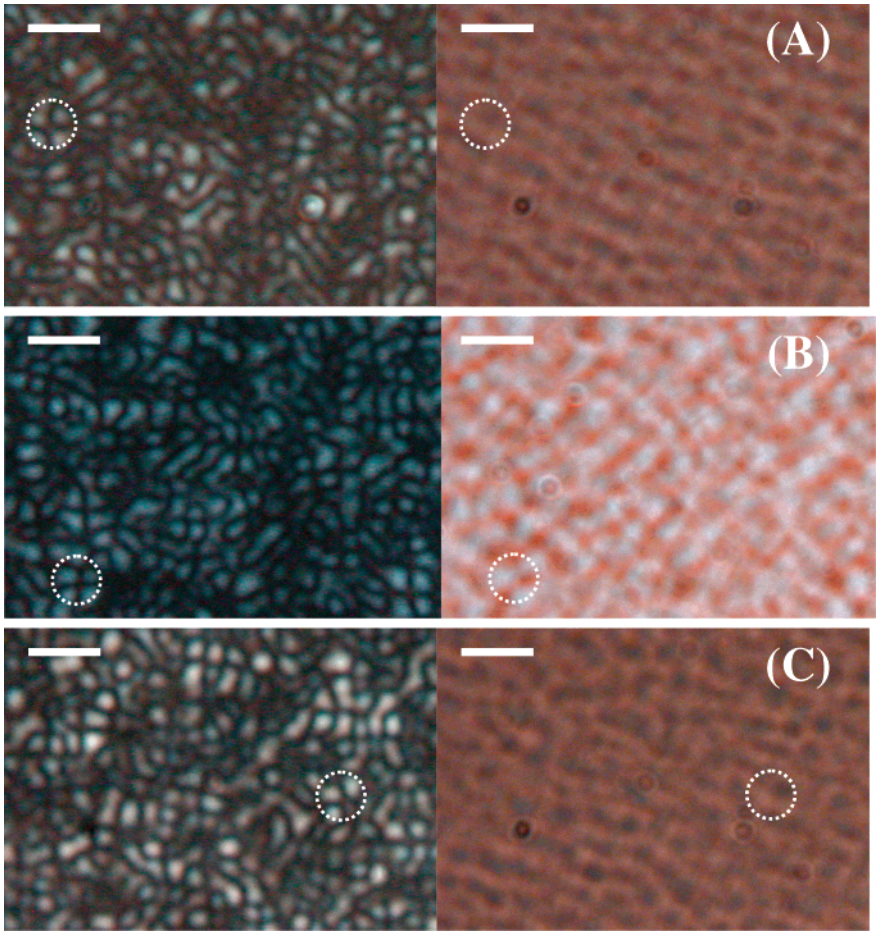

Figure 8. Typical morphological features of sPS/aPS blends observed by POM at room temperature after complete cold-crystallization at different temperatures: (A) sPS/aPS-H at 120 °C, (B) sPS/aPS-M at 120 °C, and (C) sPS/aPS-L at 110 °C. Left: images for cross-polarized observations. Right: images for bright field observations. The dotted circles enclose a spherulite and the scale bar is 10 μm.

Depending on the blends, however, the modulated morphology became rather vague at 120−150 °C, compared with those at the two temperature ends (100 and 220 °C). To calculate the periodic wavelength (Λ) of the modulated structure, two-dimensional fast Fourier transforms (FFT) was carried out on the OM micrographs to obtain the spinodal rings, from which Λ was derived by $2\pi/q_m$, where q_m was the scattering vector with maximum intensities. The T_c dependence of Λ is displayed in Figure 9 together with the spherulitic diameters determined from the Hv scattering patterns. Addition of aPS component generally leads to an increase in the spherulitic diameter. With increasing T_c, both D and Λ become larger; the former is about 1.5−2.0 times larger than the latter. In contrast, Λ is essentially smaller at higher phase separation temperatures (low quench-depth) by quenching from above UCST.[10,11] It's well-known that the driving force for the coarsening of the separated domains is the σ/η ratio, where σ is the interfacial tension between the coexisting phases and η is the effective viscosity of the fluid. In general, σ is the dominant factor for SD induced from the temperatures above UCST; whereas η becomes a determining parameter for SD induced the glassy state due to the significant reduction of chain mobility. Our results suggest that different governing factors play a determining role in the coarsening process of SD induced either from the melt or the melt-quenched glassy sate. On the basis of our OM observations, we conclude that SD phase separation spreads out the whole sample first to produce the sPS-rich and sPS-poor domains, followed by crystallization of sPS initiating in the sPS-rich domains. The developing sPS spherulites may grow across the phase boundary

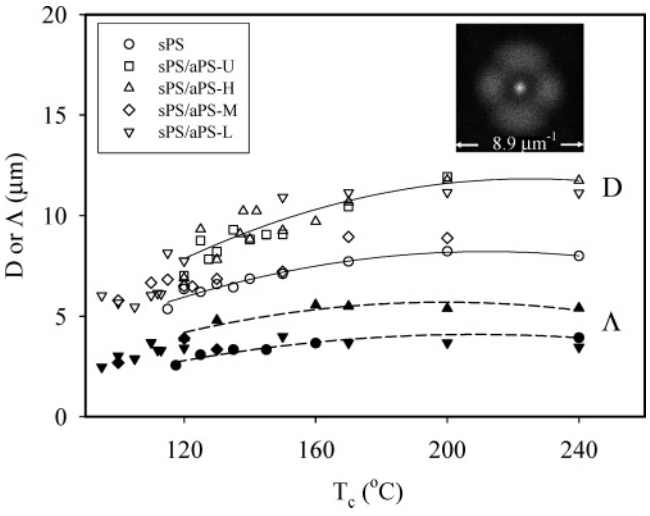

Figure 9. T_c dependence of spherulitic diameter, D, and periodic wavelength, Λ, of phase-separated structure. Open symbols denote D, and filled symbols denote Λ. The inset is a typical 2D-FFT pattern of sPS/aPS-M blends crystallized at 127.5 °C.

in the absence of altering the phase-separated structure due to the limited mobility at low T_c, leading to a SD feature conserved inside the spherulites as observed. In contrast, melt crystallization only produces spherulitic (or axilitic) morphology in the absence of any phase-separated signature[7,8] due plausibly to the significant chain rearrangement at the L−L phase boundary. Moreover, it's generally known that, in a binary blend the UCST will become lower when the MW of either one constituent is

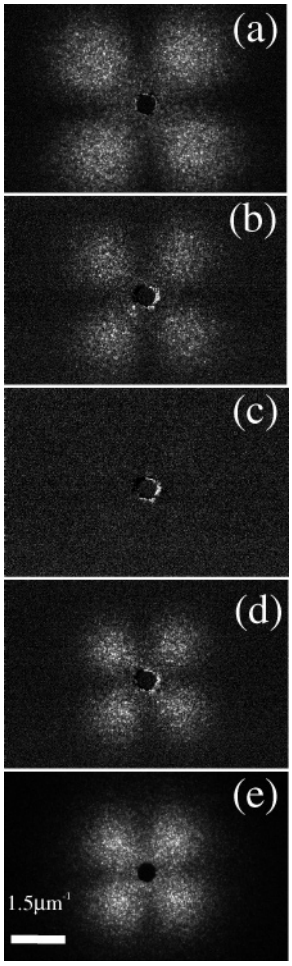

Figure 10. Typical Hv scattering patterns of completely crystallized sPS/aPS-H blends at various T_c (a) 120, (b) 130, (c) 150, (d) 160, and (e) 200 °C.

reduced, suggesting the variation of phase diagrams for our sPS/aPS blends studied. Since the SD structure is still observed for all blends cold-crystallized at a temperature as high as 240 °C (Figure 9), we conclude that the plausible UCST of the sPS/aPS blends lie between 240 and 280 °C in consideration of previous results obtained from melt crystallization as well.

Figure 10 shows the change of Hv scattering patterns taken at room temperature for the sPS/aPS-H blends after complete crystallization at the given T_c. It is of interest to note that the symmetric four-leaf-clover pattern, indicative of a spherulitic morphology, is observed at both low- and high-T_c ends, whereas barely discernible four-leaf-clover pattern is detected at 150 °C. To quantitatively characterize the spherulites developed at each T_c, the Hv invariants of completely crystallized samples (Q_m) were determined. The T_c dependence of Q_m is given in Figure 11, where a pronounced minimum is observed at an intermediate temperature (T_{min}) with a magnitude of Q_m being ca. 100 times less than those at both low- and high-temperature ends (note the logarithmic scale used for the vertical axis). Similar trends were also obtained for other blends as well as the neat sPS. The curves in Figure 11 have been vertically shifted for a clear presentation, and the T_{min} at which Q_m is minimum is 150, 150, 146, 135, and 120 °C for the neat sPS, sPS/aPS-U, sPS/aPS-H, sPS/aPS-M, and sPS/aPS-L, respectively. It seems that T_{min} shifts to a lower temperature for blends with a lower T_g.

When isothermal crystallization was completed, the spherulites became volume filling, i.e., $\phi_{sp} = 1.0$, for all the blends except the sPS/aPS-L blend, of which a small gap exists between

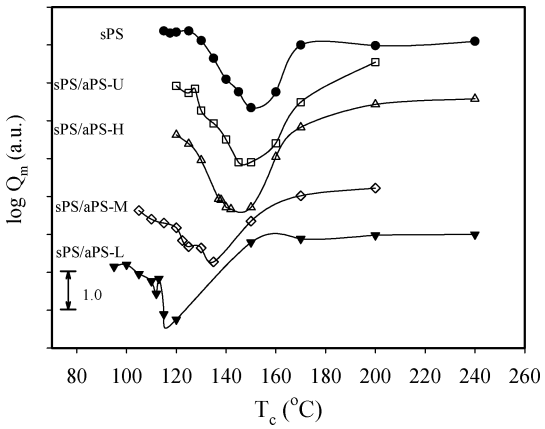

Figure 11. T_c dependence of Hv invariant of sPS/aPS blends after complete crystallization.

spherulites, according to our POM (Figure 8) and SEM observations (Figure 14, discussed later). On the basis of eq 2, Q_m becomes mainly dependent upon three factors, i.e., δ_{cr}^o, $\phi_{c,sp}$, and P_2. To distinguish individual effect on the measured Q_m, sample crystallinity and crystal modification were determined by FTIR and the results were presented in the next section.

Sample Crystallinity and Crystal Modifications. The crystallinity and crystal modification of the crystallized samples were mainly characterized by FTIR instead of using wide-angle X-ray diffraction (WAXD), by which the short-range crystal order developed normally in the cold-crystallized sPS/aPS blends might not be detected appropriately. Figure 12 shows the FTIR spectra of sPS/aPS bends cold-crystallized at various T_c. The absorbance peaks at 902 and 911 cm^{-1} are due to the α- and β-form crystals respectively, and the 906 cm^{-1} peak is associated with the amorphous phase.[27,28] For all the samples studied, mesomorphic phase of sPS was found at T_c close to T_g, judging from the presence of absorbance peaks at 1224 and 906 cm^{-1},[28] and in the absence of any sharp diffraction peaks in the WAXD patterns except a huge hump at $2\theta \sim 20°$ (not shown here). The temperature range for mesomophic-phase formation, ca. $T_g \sim T_g + 40$ °C, was dependent upon the blend mobility. For blends crystallized at higher T_c, however, the crystal modification was dependent upon the MW of aPS used. Addition of either aPS-U or aPS-H produces the α-form sPS only at 145 °C, but small trace of β-form sPS is also detected at elevated temperatures, i.e., 200 °C, as shown in Figure 12, parts a and b, by the appearance of the absorbance shoulder at 911 cm^{-1}. A similar T_c dependence of crystal modification was obtained for the neat sPS.[14] In contrast, only β-form sPS is found at T_c higher than 160 °C for the sPS/aPS-M and sPS/aPS-L blends as shown in Figure 12 c,d. It seems that β-form sPS becomes dominant crystal modification at high T_c for the blends with low MW aPS. Nevertheless, either mesomorphic or α-form sPS are developed in the temperature range where the Q_m minimum is discernible (Figure 11) for all the samples studied. It has been shown that the mesomorphic form of sPS indeed is constituted of small and imperfect crystals of the α crystalline form[28] possessing only short-range order in the absence of long-range order, suggesting that both mesomorphic and α-form sPS possess an identical δ_{cr}^o. Thus, the existence of Q_m minimum at T_{min} is attributable to the development of spherulites with a low crystallinity and/or a low degree of lamellar orientations inside.

Figure 13 shows the T_c dependence of sample crystallinities estimated by the $A_{1222\ cm^{-1}}/A_{1601\ cm^{-1}}$ ratio obtained from FTIR results. For the neat sPS, the crystallinity remains unchanged

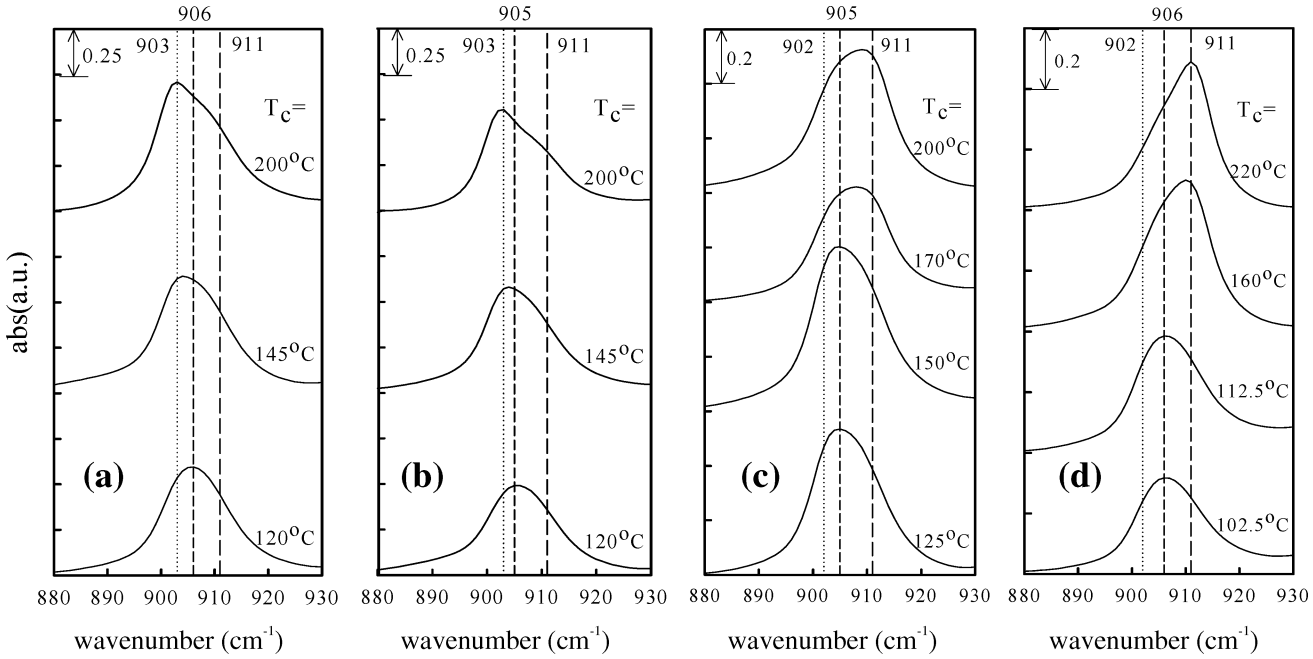

Figure 12. FTIR spectra of sPS/aPS blends cold-crystallized at various T_c, (a) sPS/aPS-U, (b) sPS/aPS-H, (c) sPS/aPS-M, and (d) sPS/aPS-L.

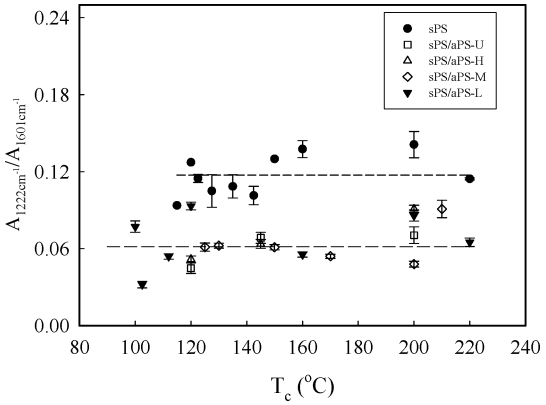

Figure 13. T_c dependence of the reduced absorbance of sPS/aPS blends measured by FTIR after complete cold crystallization. The reduced absorbance, $A_{1222\ cm^{-1}}/A_{1601\ cm^{-1}}$, represents the relative crystallinity of the sample.

despite the wide temperature range. It is consistent with WAXD results[14] and previous findings by Musto et al.[20] Although different MW of aPS and T_c were used, all sPS/aPS blends with a composition of 5/5 wt ratio possessed a similar crystallinity, as revealed by the half value of $A_{1222\ cm^{-1}}/A_{1601\ cm^{-1}}$ of the neat sPS. On the basis of FTIR results, both $\delta_{cr}{}^{o}$ and $\phi_{c,sp}$ can be assumed to be intact for those samples cold-crystallized at a temperature not far from its T_g. According to eq 2, therefore, the existence of Q_m minimum (Figure 11) is merely associated with a significant reduction of P_2, implying that the spherulites developed at T_{min} possess a much randomized lamellar orientation.

Competition between Phase Separation and Cold Crystallization. Provided that the miscible state of sPS/aPS blends at 300 °C was preserved on rapid quenching to temperatures far below its UCST, the melt-quenched blends were homogeneous and amorphous. The preservation of the miscible state has been verified by OM, SEM, FTIR, WAXD and enthalpy relaxation via DSC techniques.[2] On rapidly heating to a given T_c above T_g, the melt-quenched blends will first be demixed to various stages since there is no energy required for SD phase separation. Thus, under OM observations the SD structure should be readily observed prior to the sPS crystallization. However, the SD was difficult to recognize in the initial period until crystallization was just about to initiating, simultaneously at that moment bicontinuous phase structure was seen to spread out the whole samples. The sudden appearance of bicontinuous phase structure is indicative of SD phase separation. The difficulty in observing the initial SD prior to crystal nucleation is attributed to the low contrast between phases due to the proximity of refractive index between sPS and aPS components. The phase contrast of the bicontinuous structure is significantly enhanced when small amount of crystals form in the sPS-rich domains. Moreover, the sPS spherulites nucleating in the sPS-rich domains are growing gradually and finally crossing the phase boundary and into the aPS-rich domain without significantly altering the SD structure.

The resulted morphology of the cold-crystallized sPS/aPS is the outcome of the interplay of two kinds of phase transitions, i.e., L−L phase separation and L−S crystallization.[9−13] For example, as the amorphous quenched sPS/aPS-H blends are subsequently heated to a temperature slightly higher than T_g (T_c = 115−125 °C), limited mobility is just sufficiently high for the spontaneous SD process to take place. Thus, the early stage of SD process starts at the very initial period immediately after the desired T_c is reached, providing coexisting phases of sPS-rich and aPS-rich domains. At this stage, the phase contrast is too low to observe morphological features under OM until crystallization is about to be initiated. Late stage of SD is discernible due to the growth of oriented domains through cooperative motion of neighboring domains. Despite that insignificant coarsening of the interconnected domains is seen due to the high viscosity, the ordering process in the sPS-rich phase is prevailing, and eventually triggers the formation of stable sPS crystal nuclei. Subsequent growth of lamellar crystals spreads across the phase boundary and the signature of SD is conserved within the spherulites developed since large-scale interchain motion at the crystal front is limited at low T_c. In other words, SD phase transition dominates the morphological development.

At high T_c (170−240 °C), however, the late stage of SD is hardly discernible since a fast crystallization with an extremely

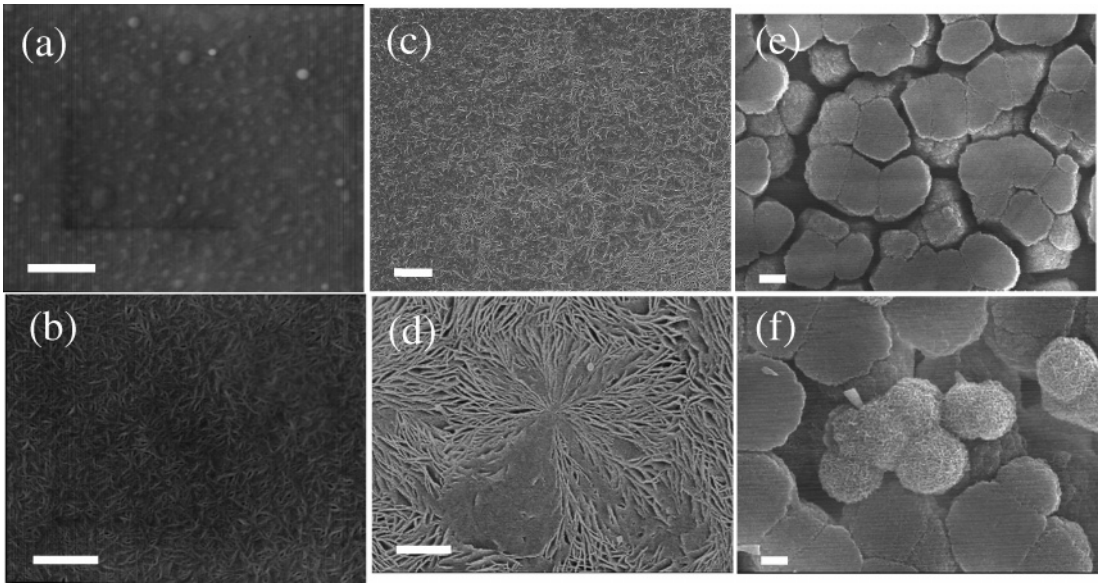

Figure 14. SEM images of sPS/aPS blends after complete cold-crystallization at various temperatures: sPS/aPS-U at (a) 120 and (b) 200 °C; sPS/aPS-H at (c) 120 and (d) 200 °C; sPS/aPS-L at (e) 95 and (f) 120 °C. Prior to SEM observation, the crystallized blends were etched using amyl acetate to extract aPS component. The scale bar is 2 μm.

short induction time takes place,[29] leading to the infeasibility of SALS for growth rate measurements. The crystallization rate is so fast that the early stage of SD may be arrested and preserved in the final morphology.[10] The crystallization becomes the dominant transition due to the enhanced chain mobility, leading to the suppression of ongoing SD coarsening process.

At the intermediate T_c (125−165 °C), the rates for the phase separation (coarsening stage) and crystallization are comparable, and these two competing processes result in the randomization of lamellar orientation within spherulites, giving rise to the Q_m minimum at 146 °C as shown in Figure 11. By adding aPS with different MW, both the coarsening rate for SD and growth rate of spherulitic (Figure 3a) are varied, thereby changing the T_{min} at which Q_m is minimum (Figure 11).

3.4. T_c Dependence of Spherulitic Growth Rate and Segregation Morphologies. The most marked change observed following the reduction in MW of aPS was the morphology of the segregated domains. Figure 14 shows SEM micrographs of sPS/aPS blends in which segregated aPS domains can be identified by the presence of voids left behind after solvent extraction. For the sPS/aPS-U blends crystallized at 120−160 °C, no apparent etched domains were observed after extensive etching of aPS using amyl acetate, indicating that the amorphous aPS-U was trapped within IL regions at low T_c (Figure 14a). The protruded granules could be the center of the spherulites. Partially IF segregation is found for sPS/aPS-U at 200 °C as shown in Figure 14b by the presence of tiny etched domains, but the IL segregation still dominates. For the sPS/aPS-H blends, IL segregation is the dominant mode at low T_c along with some aPS-H molecules residing between lamellar stacks (Figure 14c), but IF segregation becomes prevailing at high T_c (Figure 14d). For the sPS/aPS-L blend, on the other hand, the aPS-L chains are preferentially expelled to the spherulite periphery during sPS crystallization, and are confined between sPS spherulites regardless of T_c used, leading to an IS segregation morphology (Figure 14e,f). Our results are consistent with previous reports[30] that, in the weakly interacting systems, the glass transition temperature of the diluent plays an important role in determining the segregation mode during the solidification of the crystallizable component. It is frequently reported that the IS segregation mode is often accompanied by a nonlinear crystal growth as observed by POM for melt crystallization at high temperatures.[8,30] For cold crystallization, however, it is intriguing to note that a linear relation between measured R and elapsed time is still observed in the sPS/aPS-L blend in the T_c range of 95−120 °C (Figure 3a).

The segregation mode developed in a blend can be relatively defined by a δ (=D/G, where D is the diffusivity of the diluent) parameter suggested by Keith and Padden.[31] It is rationalized to expect that IL mode prevails for δ close to the amorphous layers in the long period, IF mode is for δ close to the lamellar stacks and IS mode is for δ close to the spherulitic diameter. In general, D is essentially dependent upon T_g (or MW), temperature and mixed phase composition in the vicinity of the crystal growth front. Because of the absence of specific interaction between the aPS and sPS molecules, the composition dependence of the aPS mobility was tentatively neglected, and merely the temperature and MW dependence were considered. We assumed that the temperature dependence of D obeys the Arrhenius relation with an activation energy of ca. 90 kJ/mol for the aPS component.[32,33] Moreover, the self-diffusion coefficient of aPS has been experimentally shown to be inversely proportional to the square of the MW[33−35] although theoretical prediction suggests a different MW dependence above and below the critical molecular weight for entanglements. On the basis of these assumptions, the calculated D increases with increasing T_c, but the MW dependence exhibits a more pronounced effect.[8] By varying the MW of aPS diluents, an extensive D range from $\sim 10^{-16}$ cm^2/s for aPS-U at 100 °C to $\sim 10^{-7}$ cm^2/s for aPS-L at 250 °C is obtained to test the relevance of the δ parameter. Figure 15a shows the variation of G with T_c for various blends either cold-crystallized at low temperatures (90−160 °C) or melt-crystallized[7,8] at high temperatures (240−270 °C). In the T_c range between 160 and 230 °C, G measurements become infeasible due to the rapid crystal growth prior to reaching the target temperature. In the processing window for crystallization ($T_g \sim T_m^o$), a maximum in G with the crystallization temperature is observed. The temperature at which G is maximum is lower as the aPS-L component is used. For the sPS/aPS blends, it should be noted that melt crystallization produces β-form sPS,[18] but meso-form (or imperfect α-form) sPS crystals are developed via cold crystallization in

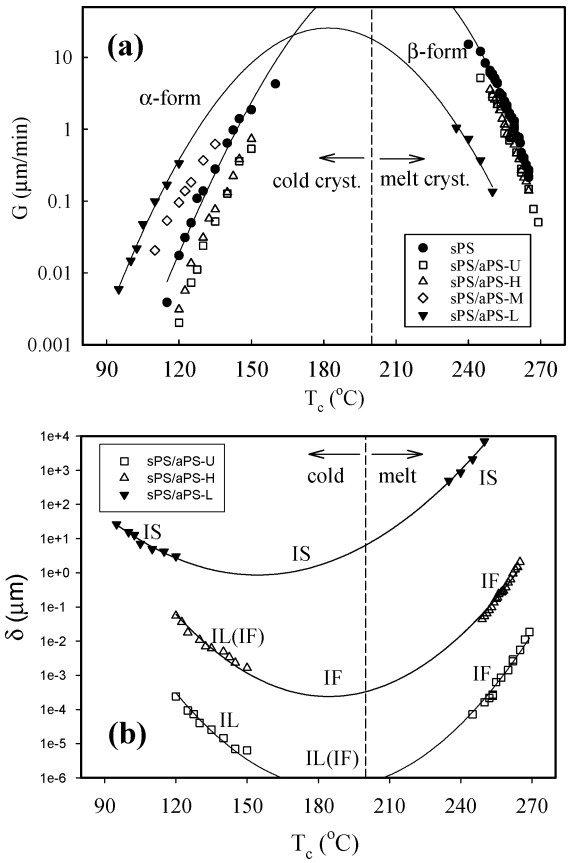

Figure 15. T_c dependence of (a) measured crystal growth rate G and (b) calculated segregation length δ. Data above 200 °C are obtained from the melt-crystallization results,[8] and solid lines are the second order regression fits for the eye-guide only. IS, IF, and IL denote the interspherulitic, interfibrillar, and interlamellar segregation mode, respectively, observed by SEM, and the segregation mode in the parentheses shows the presence of the minor morphology.

the T_c range (Figure 12). Since the crystal modification is different from each other in these two groups, the Lauritzen−Hoffman−Miller kinetic theory used conventionally for the growth rate analysis is not applicable to the whole T_c range. To estimate the maximum growth-rate temperature, a second-order regression was conducted to include all G values for the given sample and the results showed: ~200 °C for the neat sPS, and ~182 °C for the sPS/aPS-L blend having the lowest T_g and T_m^o. Using the growth rate data in Figure 15a, the derived segregation length (δ) as a function of T_c is plotted in Figure 15b for various blends, and the segregation mode is marked as well according to SEM results. Since D increases monotonically with T_c, the presence of δ minimum[36] is attributed to the maximum in G at an intermediate temperature. Experimentally, it is seen that IS mode is favored in the sPS/aPS-L blends regardless of the extensive T_c range used. This is in accordance with the theoretical considerations; the derived δ value (5−5000 μm) is larger than the spherulitic diameter (5−20 μm). On the basis of Figure 15b, it is likely that the segregation mode transition from IS to IF takes place at $\delta \sim 1$ μm. For the sPS/aPS-U blend, on the other hand, increasing T_c (from low to high) gives rise to IL, mixed IL/IF, and finally IF segregation mode at temperatures above 250 °C. In consideration of the minimum for δ around 190 °C, however, the mixed segregation mode should be prohibited intuitively. Moreover, IL segregation is still not a dominant mode in the melt-crystallized sPS/aPS-U blends although the estimated δ parameter is as low as 1 nm, which is smaller than the thickness of amorphous layers between crystalline lamellae, ~ 7 nm.[18] More importantly, at a given δ value the segregation mode induced from the glass and melt are different from each other, suggesting that other factors should be involved in predicting the segregation morphology accurately. The discrepancy might be associated with the difficulty in determining the precise aPS diffusivity, despite the fact that the intermolecular interaction between the aPS and sPS components is absent in our blends. In addition, the stiffness of the crystallizable chains and the process of lamellar growth have also been suggested to ultimately define the blend morphology.[37] In fact, lamellae with short lateral dimensions are found in the cold-crystallized sPS[14] in contrast with those developed in the melt-crystallized sPS where long and parallel lamellae are detected.[18] Thus, during cold crystallization the amorphous aPS-U (or aPS-H) chains are readily trapped between the relatively random and segmented lamellae; whereas melt crystallization produces long and rigid lamellar bundles to expel the mobile aPS effectively to the IF regions. These observations lead us to conclude that the δ parameter should be considered a qualitative expression for the segregation mode unless a precise mutual diffusivity of the diluents and detailed growth mechanism are provided.

4. Conclusions

Our studies were concerned with the MW effects of aPS on the crystallization kinetics, phase structure, crystal modification and segregation morphologies of sPS/aPS blends induced from the glassy state using SALS, SEM, OM, and FTIR. In addition, we have paid special attention to the relative relevance and interplay of the two phase transitions, i.e., L−L phase separation and L−S cold crystallization.

By plotting the normalized growth rate vs $T_c - T_g$, it was of importance to notice that all the data were superimposed upon a "master curve" except the sPS/aPS-L blend, suggesting a different growth mechanism for the sPS/aPS-L blend from the others. Because of the enhanced mixing entropy, an additional energy was required in the sPS/aPS-L blend than in other blends for the sPS segments to demix and diffuse to the crystal growing front, which in turn gave rise to the interspherulitic segregation of aPS-L component as revealed by SEM. By controlling the aPS MW and crystallization temperatures, distinct differences in the segregation morphology (either IL, IF, IS, or mixed) were obtained. For all the cold-crystallized sPS/aPS blends as well as the neat sPS, T_c dependence of Q_{Hv} exhibited a pronounced minimum at an intermediate temperature between 100 and 170 °C, and the corresponding temperature was relevant to the blend mobility. SD phase separation was evidenced by the interconnected domain structure preserved within the developed spherulites as reveled by the phase contrast microscopy. Since the crystallinity and crystal modification of the blends remained relatively unchanged regardless of the T_c used, the presence of the Q_{Hv} minimum was attributed to the randomization of sPS lamellae developed within spherulites, resulting from a comparable competition between cold crystallization and SD phase separation. The former was dominant at high T_c but the later became dominant at low T_c, leading to the development of spherulites with a more ordered symmetry inside at both temperature ends.

Acknowledgment. The authors are grateful to the National Science Council of Taiwan (ROC) for the research grant (NSC93-2218-E-006-008).

References and Notes

(1) Bonnet, M.; Buhk, M.; Trogner, G.; Togausch, K. D.; Petermann, J. *Acta Polym.* **1998**, *49*, 174.

(2) Hong, B. K.; Jo, W. H.; Kim, J. *Polymer* **1998**, *39*, 3753.
(3) Woo, E. M.; Lee, M. L.; Sun, Y. S. *Polymer* **2000**, *41*, 883.
(4) Chiu, F. C.; Peng, C. G. *Polymer* **2002**, *43*, 4879.
(5) Park, J. Y.; Kwon, M. H.; Park, O. O. *J. Polym. Sci., Part B: Polym. Phys.* **2000**, *38*, 3001.
(6) Wu, F. S.; Woo, E. M. *Polym. Eng. Sci.* **1999**, *39*, 825.
(7) Wang, C.; Liao, W.-P.; Wang, M.-L.; Lin, C.-C. *Polymer* **2004**, *45*, 973.
(8) Wang, C.; Wang, M.-L.; Fan, Y.-D. *Macromol. Chem. Phy.* **2005**, *206*, 1791.
(9) Chen, H.-L.; Hwang, J. C.; Yang, J.-M.; Wang, R.-C. *Polymer* **1998**, *39*, 6983.
(10) Inaba, N.; Sato, K.; Suzuki, S.; Hashimoto, T. *Macromolecules* **1986**, *19*, 1690.
(11) Shimizu, K.; Wang, H.; Wang, Z.; Matsuba, G.; Kim, H.; Han, C. C. *Polymer* **2004**, *45*, 7061.
(12) Zhang, X.; Wang, Z.; Muthukumar, M.; Han, C. C. *Macromol. Rapid Commun.* **2005**, *26*, 1285.
(13) Zhang, X.; Wang, Z.; Dong, X.; Wang, D. Han, C. C. *J. Chem. Phys.* **2006**, *125*, 024907.
(14) Wang, C.; Lin, C.-C.; Chu, C.-P. *Polymer* **2005**, *46*, 12595.
(15) Matsuba, G.; Kaji, K.; Nishida, K.; Kanaya, T.; Imai, M. *Macromolecules* **1999**, *32*, 8932.
(16) Olmsted, P. D.; Poon, W. K.; McLeish, T. C. B.; Terrill, N. J.; Ryan, A. J. *Phys. Rev. Lett.* **1998**, *81*, 373.
(17) Phillips, R. A. *J. Polym. Sci., Part B: Polym. Phys.* **2000**, *38*, 1947.
(18) Wang, C.; Liao, W.-P.; Cheng, Y.-W.; Lin, T.-L. *Polymer* **2004**, *45*, 961.
(19) Reynolds, N. M.; Stidham, H. D.; Hsu, S. L. *Macromolecules* **1991**, *24*, 3662.
(20) Musto, P.; Tavone, S.; Guerra, G.; De Rosa, C. *J. Polym. Sci., Part B: Polym. Phys.* **1997**, *35*, 1055.
(21) Kit, K. M.; Schultz, J. M. *J. Polym. Sci., Part B: Polym. Phys.* **1998**, *36*, 873.
(22) Stein, R. S.; Thodes, M. B. *J. Appl. Phys.* **1960**, *31*, 1873.
(23) Suzuki, T.; Kovacs, A. J. *Polymer J.* **1970**, *1*, 82.
(24) Koberstein, J.; Russell, T. P.; Stein, R. S. *J. Polym. Sci., Part B: Polym. Phys.* **1979**, *17*, 1719.
(25) Avrami, M. *J. Chem. Phys.* **1930**, *7*, 1109.
(26) Okamoto, M.; Inoue, T. *Polymer* **1995**, *36*, 2739.
(27) Sun, Y. S.; Woo, E. M.; Wu, M. C.; Ho, R.-M. *Macromolecules* **2003**, *36*, 8415.
(28) Auriemma, F.; Petraccone, V.; Poggeto, F. D.; De Rosa, C.; Guerra, G.; Mafredi, C. *Macromolecules* **1993**, *26*, 3772.
(29) Matsuba, G.; Kaji, K.; Kanaya, T.; Nishida, K. *Phys. Rev. E* **2002**, *65*, 061801.
(30) Wu, L.; Lisowski, M.; Talibuddin, S.; Runt, J. *Macromolecules* **1996**, *29*, 1576.
(31) Keith, H. D.; Padden, F. J. *J. Appl. Phys.* **1964**, *35*, 1270.
(32) Tirrell, M. *Rubber Chem. Technol.* **1984**, *57*, 523.
(33) Fleischer, G. *Polym. Bull. (Berlin)* **1983**, *9*, 152.
(34) Bachus, R.; Kimmich, R. *Polymer* **1983**, *24*, 964.
(35) Graessley, W. W. *J. Polym. Sci., Polym. Phys. Ed.* **1980**, *18*, 27.
(36) Hsiao, B. S.; Sauer, B. B. *J. Polym. Sci., Polym. Phys. Ed.* **1993**, *31*, 901.
(37) Debier, D.; Jonas, A. M.; Legras, R. *J. Polym. Sci., Polym. Phys. Ed.* **1998**, *36*, 2197.

MA061159K